

Visual Adaptive Prompting for Compositional Zero-Shot Learning

Kyle Stein¹, Arash Mahyari^{1,2},
Guillermo Francia, III ³, **Eman El-Sheikh** ³

¹Department of Intelligent Systems and Robotics, University of West Florida, Pensacola, FL, USA

²Florida Institute For Human and Machine Cognition (IHMC), Pensacola, FL, USA

³Center for Cybersecurity, University of West Florida, Pensacola, FL, USA

Corresponding Author: ks209@students.uwf.edu

This work is partially supported by the UWF Argo Cyber Emerging Scholars (ACES) program funded by the National Science Foundation (NSF) CyberCorps® Scholarship for Service (SFS) award under grant number 1946442. Any opinions, findings, and conclusions or recommendations expressed in this document are those of the authors and do not necessarily reflect the views of the NSF.

ABSTRACT Vision-Language Models (VLMs) have demonstrated impressive capabilities in learning joint representations of visual and textual data, making them powerful tools for tasks such as Compositional Zero-Shot Learning (CZSL). CZSL requires models to generalize to novel combinations of visual primitives—such as attributes and objects—that were not explicitly encountered during training. Recent works in prompting for CZSL have focused on modifying inputs for the text encoder, often using static prompts that do not change across varying visual contexts. However, these approaches struggle to fully capture varying visual contexts, as they focus on text adaptation rather than leveraging visual features for compositional reasoning. To address this, we propose *Visual Adaptive Prompting System* (VAPS) that leverages a learnable visual prompt repository and similarity-based retrieval mechanism within the framework of VLMs to bridge the gap between semantic and visual features. Our method introduces a dynamic visual prompt repository mechanism that selects the most relevant attribute and object prompts based on the visual features of the image. Our proposed system includes a visual prompt adapter that encourages the model to learn a more generalizable embedding space. Experiments on three CZSL benchmarks, across both closed and open-world scenarios, demonstrate state-of-the-art results.

INDEX TERMS Compositional Zero-Shot Learning, Soft Prompting, Vision Language Models.

I. INTRODUCTION

HUMANS have a remarkable ability to compose attributes with objects to imagine novel combinations they have never encountered, for example, a blue banana. Attributes describe the state of an object, such as the color, texture, or shape, while objects represent the entities themselves, such as a banana or a car. This ability to associate various attributes with different objects is a fundamental aspect of human cognition, known as compositionality [1]–[3]. Compositional Zero Shot Learning (CZSL) aims to mimic this human behavior by enabling models to recognize combinations of primitive attributes and objects that were not explicitly composed, or seen together, during training. CZSL focuses on the recombination of known primitives, allowing for the recognition of novel compositions by effectively dis-

entangling attribute and object information from a combined visual representation [4]–[6].

The rigorous pre-training of VLMs have shown great ability for understanding tasks that require both visual and textual data. Models like CLIP [7] are trained on vast amounts of image-text data and learn to map visual and textual concepts into a shared embedding space, enabling them to perform tasks such as zero-shot classification and image recognition. However, when approached with the more nuanced understanding of compositional reasoning, CLIP lacks the ability to generalize to unseen primitive compositions. This lack of generalization can be attributed to the reliance on static representations of fixed classes seen during training and the lack of flexibility to adjust their internal prompts to changes in visual inputs [8]–[10].

Recent studies in CZSL based on VLMs [11]–[13] suffer from several drawbacks which limit their performance. **First**, state-of-the-art (SOTA) methods typically utilize either fixed templates “a photo of [attribute][object]” or a single learned prefix prepended to “[attribute][object]”. In these strategies, the text prompt is processed through the text encoder, while the raw image is handled by the image encoder, leading to the development of a joint embedding that facilitates the inference of unseen attribute-object compositions. Although promising, text-focused methods largely overlook valuable visual insights, as they concentrate on tuning text-based prompts rather than exploiting visual information that could enhance attribute-object disentanglement and improve model adaptability to unseen compositions [14], [15]. **Second**, SOTA algorithms typically rely solely on these text-centric learnable prompts. and operate under the assumption that a minimal number of prompts can adequately capture all attribute-object combinations. For example, a single prompt might be used to denote a variety of attributes like “wet,” “dry,” “red,” etc. This limited approach constrains the development of tailored prompts that could significantly improve performance. Moreover, using only one or two prompts means these techniques struggle to properly separate attribute features from object features, thereby restricting their effectiveness in generalizing to unseen compositions. **Third**, text-centric approaches utilize fixed prompts as a prefix to “[attribute][object]” during training. These *static prompts* are comprised of a set of learnable variables that remain constant in their positions across different attribute-object pairings, such as transitioning from “wet cat” to “red apple”. Relying on such static, learnable text prompts often fails to fully encompass the entire context of an image. This is because text descriptions can be relatively rigid, not adequately reflecting the complexities of an image. For instance, the attribute “wet” might carry different semantic implications when associated with disparate objects like a cat versus an apple.

To address these challenges, we propose a novel approach *Visual Adaptive Prompting System (VAPS)* that builds on CLIP’s multi-modal architecture by leveraging a dynamic visual prompt repository and a similarity-based retrieval mechanism, which shifts the emphasis to the image features generated by CLIP’s visual encoder. VAPS creates a repository of visual features to serve as visual prompts, comparing them with fused features in a pair space, as well as implementing a prompt adapter based on the original image features that allows the model to adapt its representation based on the visual context. The summary of our contributions for CZSL are stated below:

- **Visual Prompts:** To leverage information directly from the image encoder, we introduce visual prompts. These visual prompts are learnable embeddings designed to capture visual patterns related to attributes and objects. This high-level semantic representation efficiently separates attributes from object visual features, allowing

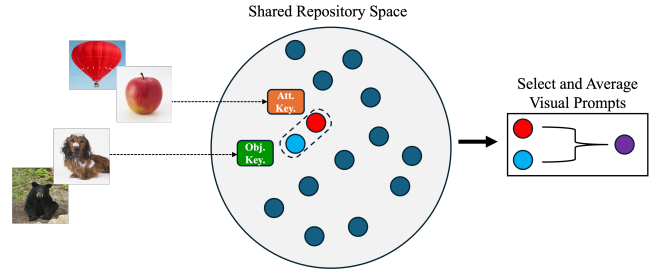


FIGURE 1. Similarity-Based Visual Repository Mechanism. The image features are matched against learned keys in a shared repository space, where similarity scores are computed. Based on these similarity scores, the most relevant learned visual prompts representing attributes (i.e., “color”) and objects (i.e., “animals”) are selected. The selected prompts are then averaged, creating a final representation (purple) that holds the object and attribute information of the input images. This process allows dynamic retrieval and combination of relevant visual prompts for downstream tasks.

VAPS to generalize visual semantics to unseen compositions more effectively. Unlike text-based prompts, visual prompts leverage visual features to enhance disentanglement and boost adaptability.

- **Prompts Repository:** Our approach employs a repository of learnable visual prompts that operate independently from those used by the text encoder. Each visual prompt in this repository is paired with a learnable key, which serves as an identifier for effective selection. VAPS uses a similarity-based retrieval mechanism to match image features with learned keys in the repository, selecting the most relevant prompts for the input image. This allows the model to effectively disentangle attributes from objects, facilitating generalization to unseen compositions.
- **Text Prompt Adapter:** VAPS incorporates an adapter that dynamically updates the prefix of the text prompt using image features from the visual transformer. By incorporating a bias term from image features, this approach customizes the prompt for each image, aligning it with the visual context and effectively separating attributes from objects. For instance, the learnable text prompts are adjusted with different bias values when processing images of a “wet cat” versus a “red apple,” overcoming the limitations associated with *static prompts*.

II. Related Work

Compositional Zero-Shot Learning extends the principles of zero-shot learning by focusing on the recognition of unseen compositions of known primitives. As previously mentioned, disentanglement is a prevalent approach in many CZSL methods [4], [16]–[18]. However, this is not the only approach to achieve compositional generalization. Li et. al. uses the principles of symmetry and group theory to model attribute-object compositions through coupling and decoupling transformations, and introduces a novel distance method for CZSL [19]. A Siamese Contrastive Embedding Network (SCEN) embeds visual features into a siamese

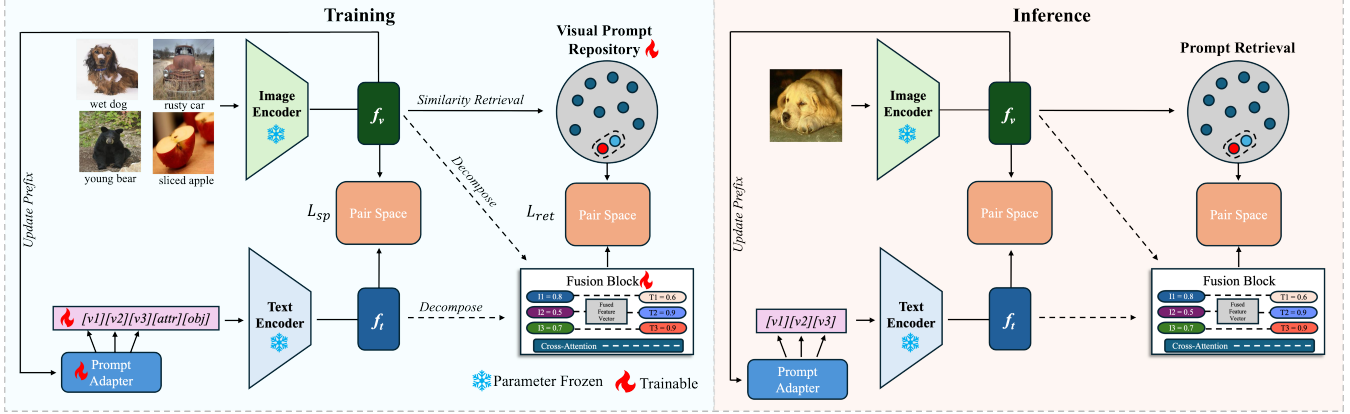


FIGURE 2. VAPS harnesses the power of CLIP as its backbone. Our groundbreaking approach addresses this by freezing CLIP’s pre-trained visual and text encoders. The input image is passed through the image encoder of CLIP to extract image features f_v . These features are used as the input to the prompt adapter to provide the bias for shifting three learnable prefix text tokens $[v1][v2][v3]$. The shifted prefix is prepended to the word embeddings of attributes and objects and passed through the text encoder of CLIP to get f_t . For each input image, the similarity of f_v is compared with all visual prompts in the repository and the two top most similar visual prompts are retrieved and averaged. Then, f_v and f_t are decomposed and fused, where the output is mapped with the average of the selected visual prompts in a dedicated pair space. Additionally, $f_v \in \mathbb{R}^{768}$ represents the text feature extracted by the text encoder. Both are separately mapped onto another pair space. During inference, all steps are taken except that the learned prompt network shifts the three prefix text prompts $[v1][v2][v3]$. The final logits are computed based on the similarity between image and text features in the pair space, as well as the similarity between the averaged visual prompts and the outcome of the fusion block. The aggregated logits are used to determine the final predicted composition, selecting the attribute and object with the highest score for the test image.

contrastive space to separately capture attribute and object prototypes diversity [20]. A retrieval-augmented approach was proposed to enhance the recognition of unseen primitive compositions by retrieving and augmenting attribute and object representations [21]. Wang et. al. propose a dependent approach for CZSL that generates conditional attribute embeddings by using an attribute hyper learner and base learner to account for the varying interaction of attributes with different objects [22].

Modern applications in CZSL include adapting pre-trained VLMs, such as CLIP [7], to improve CZSL results. It is shown that downstream tasks can be built on top of the VLMs to enhance these results. Compositional Soft Prompting (CSP), introduced in [23], uses a static prompt prefix combined with learned attribute and object descriptions. This text is passed through a text encoder while the image is processed by CLIP’s visual encoder. The model then calculates the cosine similarity between the text embeddings and image features to predict the correct attribute-object composition. More recent works built on top of this method by removing the static prefix content and instead making the entire prompt learnable [11], [13]. While these processes produce promising results, only one learned prompt may not generalize well to every image passed through the visual encoder.

Prompt Learning/Tuning modifies the original input by leveraging learnable tokens that guide the pre-trained language model to examine specific features or contexts relevant to the task the model is trying to solve [24]–[26]. With the more recent advancements in VLMs, prompt learning has steered into a new direction by focusing on the multimodality of both textual and visual content in a shared

embedding space [7], [27], [28]. Huang et. al. introduced a method to transfer performance from VLMs without the need for prompt engineering or labeled data by generating pseudo labels for target datasets and optimizing learnable prompt representations through self-training on the psuedo-labeled samples [29]. Prompt learning has been applied on top of pre-trained vision transformers to solve the catastrophic forgetting problem in continual learning by using a pool of learnable prompts to learn tasks sequentially [30]. CoOp [10] introduced a method to automate prompt engineering for models like CLIP by learning the vectors of prefix content while keeping the pre-trained model fixed for few-shot scenarios. To improve on CoOp, researchers introduced CoCoOp [31] which learns a lightweight neural network that generates dynamic prompts based on the input image.

III. Preliminaries and Insights

Let A denote the set of attributes and O denote the set of objects. Given a set of attributes $A = \{a_0, a_1, \dots, a_n\}$ and a set of objects $O = \{o_0, o_1, \dots, o_m\}$, we define the set of all possible compositions $C = A \times O$, where \times is the Cartesian product. The set C can be divided into two disjoint subsets: seen compositions C_s and unseen compositions C_u , where $C_s \cap C_u = \emptyset$ and $C_s \cup C_u = C$.

In Closed-World CZSL, the model operates under the assumption that all possible compositions for testing are drawn from a predefined subset $C_{\text{test}} \subseteq C$. This means that while some compositions may be unseen during training, they are still part of this known subset. Consequently, the test set includes both C_s and C_u , but all testing samples are limited to this established set $C_s \cup C_u$, restricting the model to a predefined range of feasible combinations. In Open-World CZSL [32], the model must navigate the

entire composition space $C = A \times O$, which includes both feasible and infeasible combinations. This presents an added challenge, as the model encounters compositions that were neither seen during training nor predefined as possible during testing, making classification more complex. The objective is to learn a function $f : X \rightarrow C_{\text{test}}$ for Closed-World settings and $f : X \rightarrow C$ for Open-World settings, where X denotes the input space of images corresponding to these compositions.

IV. Methodology

Our approach builds upon the capabilities of VLMs, such as CLIP, for compositional learning by freezing its pre-trained visual and text encoders. During training, each input image is processed through CLIP’s visual encoder to obtain feature representations f_v . These features are used two-fold: (i) as input to the text prompt adapter to find the appropriate bias for dynamically shifting a set of learnable prefix text tokens and (ii) used to select visual prompts from the repository. The shifted prefix tokens are prepended to the word embeddings of attributes and objects to form the final text prompt, which is processed through the text encoder to produce text features f_t . Next, f_v and f_t are decomposed and fused via cross-attention, resulting in a joint representation that is mapped to a dedicated pair space. In this space, the similarity between the fused representation of $\langle f_v, f_t \rangle$ and the selected visual prompts informs the final compositional prediction. Additionally, both f_v and f_t are each projected into a separate pair space to facilitate the compositional prediction.

During inference, the same processing pipeline is followed with one main difference: ground truth attribute-object pairings are unavailable. Instead, text prompts are generated for each candidate pair $(a, o) \in C^{\text{test}}$ using the shifted prefix, and the final predicted composition is selected as the pair yielding the highest retrieval probability p_{ret} . Figure 2 provides an overview of our method.

A. Visual Prompt Repository

The visual prompt repository comprises a collection of M learnable visual prompts $\mathbf{P}_1, \mathbf{P}_2, \dots, \mathbf{P}_M$, where each $P_i \in \mathbb{R}^{l \times d}$ represents an individual visual prompt, and l denotes the prompt length. These prompts are initialized randomly and refined during training to capture high-level semantic visual features, such as colors, textures, and shapes. Each visual prompt P_i is paired with a learnable key $a_i \in \mathbb{R}^d$, which helps identify the most relevant prompts for a given image by measuring similarity between the input image features and the keys. The keys a_i are used for similarity assessment, while P_i contributes to predicting attributes and objects in the joint embedding space, combined with the output of the fusion block. To find the best-matching visual prompts, cosine similarity is computed between the normalized visual features f_v of the input image and each normalized key a_i . Based on the similarity scores, the model selects the top two prompts with the highest cosine similarity,

ensuring that one prompt aligns with the image’s attribute and the other with the object. These selected prompts are then averaged, forming a combined representation that is later integrated with the visual and textual features to improve compositional prediction. By dynamically selecting the most relevant visual prompts, the model improves image-text alignment and enriches the representation of image content. Over the course of training, each visual prompt becomes more adept at capturing the visual characteristics of basic elements, such as “red” or “wet,” enabling more precise attribute-object mapping and enhancing generalization to unseen compositions. The final representation of the retrieved visual prompts can be denoted by f_{ret} .

B. Text Prompt Adapter

In SOTA CZSL algorithms, “[attribute][object]” is prepended with learnable text soft prompts. These soft prompts typically consist of a few trainable tokens, such as three prefix tokens [v1][v2][v3], which are initialized with a generic phrase like “a photo of” to align with CLIP’s pretraining [11], [13], [23]. However, these tokens remain fixed in location and combination for every training and inference sample, making no distinction between different attributes and objects. Therefore, during inference, when “[attribute][object]” is not available, the same trained prefix text soft prompt is used for every test sample, leading to poor generalization on unseen compositions. Fig. 3 (a) illustrates this limitation, where the same prompt is applied to both “wet cat” and “red apple,” failing to account for the unique visual and semantic context of each example. To remain consistent with SOA result comparison, in our approach, three prefix tokens are initialized.

Motivated by the prompting method introduced in [31], we incorporate a prompt adapter module with trainable parameters. The prompt adapter takes the image feature f_v as the input and provides the amount of the shift for the text prompt in the output. The parameters of the prompt adapter are updated during training. Fig. 3 (b) and (c) are two examples of shifted version of Fig. 3 (a) for the example “wet cat” and “red apple”, discriminating the input to the text encoder, leading to superior performance. The prefix structure of the learnable soft prompt provides a general context for the task while the attribute and object represent the composition of the object. The prompt adapter is a lightweight neural network, represented as:

$$\text{PromptNet}(f_v) = \mathbf{W}_2 \cdot \sigma(\mathbf{W}_1 \cdot f_v + \mathbf{b}_1) + \mathbf{b}_2, \quad (1)$$

where f_v represents the visual features, \mathbf{W}_1 , \mathbf{W}_2 , \mathbf{b}_1 , and \mathbf{b}_2 represent the linear layers and their bias terms, respectively, and $\sigma(\cdot)$ is the ReLU activation function. The output of the prompt adapter network is a bias term, denoted as $\varphi(f_v)$, which is added to each of the learnable embeddings in the soft prompt’s prefix $\{\theta_0, \theta_1, \dots, \theta_p\}$. This is represented as:

$$\theta'_i = \theta_i + \varphi(f_v) \quad \text{for } i = 0, \dots, p, \quad (2)$$

where each θ'_i represents the shifted version of the original prompt embedding θ_i . Therefore, the updated shift in the

soft prompt P'_{soft} is $P'_{\text{soft}} = \{\theta'_0, \theta'_1, \dots, \theta'_p, \theta_a, \theta_o\}$. The text features f_t are obtained by passing P'_{soft} through the text encoder.

C. Decomposition and Fusion Block

To disentangle the visual features of attributes and objects and embed them jointly with their text representation, we decompose and fuse the visual features, f_v , and the text features, f_t [13]. Specifically, the text feature representation is decomposed by averaging the contributions of the attributes and objects from the corresponding logits. Decomposition helps isolate the properties of attributes and objects, allowing the model to treat these two components independently during subsequent fusion. The decomposed features are supervised during training to accurately capture the primitive's information. We compute the attribute and object probability as follows:

$$p(y = a | x; \theta) = \frac{\exp(f_v \cdot f_t)}{\sum_{a \in \mathcal{A}} \exp(f_v \cdot f_t)}, \quad (3)$$

$$p(y = o | x; \theta) = \frac{\exp(f_v \cdot f_t)}{\sum_{o \in \mathcal{O}} \exp(f_v \cdot f_t)}, \quad (4)$$

where \mathcal{A} and \mathcal{O} denote the sets of attributes and objects. The cross-entropy can be minimized as:

$$\mathcal{L}_{\text{att}} = -\frac{1}{|\mathcal{A}|} \sum_{(x,y) \in \mathcal{C}^s} \log(p(y = (a) | x; \theta)), \quad (5)$$

$$\mathcal{L}_{\text{obj}} = -\frac{1}{|\mathcal{O}|} \sum_{(x,y) \in \mathcal{C}^s} \log(p(y = (o) | x; \theta)). \quad (6)$$

Next, f_v and f_t are fused through a cross-attention mechanism, where the query (Q), key (K), and value (V) matrices focus on aligning image and text features within a compositional space. Specifically, Q is derived from f_t , while K and V are derived from f_v where the key represents the aspects of the image that the query will attend to, and the value holds the information that will be emphasized based on how well Q aligns with K . Here, d denotes the dimensionality of the feature vectors in the compositional space. The cross-attention can be computed as follows:

$$\text{Attention}(Q, K, V) = \text{softmax} \left(\frac{QK^T}{\sqrt{d}} \right) V. \quad (7)$$

This cross-attention operation yields $f_{t \rightarrow v}$, a fused representation that incorporates textual context of the attributes and objects with the visual features.

D. Training

The additional training of our model is conducted in two parts: one focuses on adapting the soft prompt to the target compositions, and the other on the alignment between retrieved prompts and the final fused representation $f_{t \rightarrow v}$. To ensure the shifted soft prompts align with the target compositions, the class probability for the soft prompt are computed as follows:

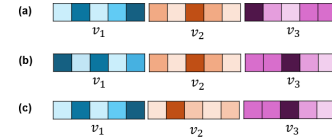


FIGURE 3. (a) The fixed, static text soft prompt used for all samples during inference in state-of-the-art (SOTA) methods. (b) and (c) Examples showing adapted (shifted) text soft prompts for two different images during inference. The shift or bias amount is determined by the prompt adapter, whose parameters are trained to identify the optimal adjustment based on the input image features.

$$p_{\text{sp}}(y = (a, o) | x; \theta) = \frac{\exp(f_v \cdot f_t)}{\sum_{(a', o') \in \mathcal{C}^s} \exp(f_v \cdot f_t)}, \quad (8)$$

where f_t is the text feature representation from the shifted soft prompt and \mathcal{C}^s denotes the set of seen compositions. To encourage the adapted soft prompt to generate text features that align with the target compositions, the cross-entropy over these probabilities is minimized to form the soft prompt alignment loss:

$$\mathcal{L}_{\text{sp}} = -\frac{1}{|\mathcal{C}^s|} \sum_{(x,y) \in \mathcal{C}^s} \log(p_{\text{sp}}(y = (a, o) | x; \theta)). \quad (9)$$

Next, we ensure that the fused features accurately reflect the retrieved prompts from the repository. The probability of this is defined as p_{ret} and apply the softmax function over \mathcal{C}^s :

$$p_{\text{ret}}(y = (a, o) | x; \theta) = \frac{\exp(f_{\text{ret}} \cdot f_{t \rightarrow v})}{\sum_{(a', o') \in \mathcal{C}^s} \exp(f_{\text{ret}} \cdot f_{t \rightarrow v})}. \quad (10)$$

The cross-entropy loss is then minimized over the class probabilities. The objective function is defined as:

$$\mathcal{L}_{\text{ret}} = -\frac{1}{|\mathcal{C}^s|} \sum_{(x,y) \in \mathcal{C}^s} \log(p_{\text{ret}}(y = (a, o) | x; \theta)). \quad (11)$$

The total loss function for training the model is then a weighted combination of the compositional, attribute, object, and soft prompt losses, where $\lambda_{\text{att_obj}}$ and λ_{sp} are hyper-parameters that control the relative weight of the attribute-object loss and the soft prompt loss:

$$\mathcal{L}_{\text{total}} = \mathcal{L}_{\text{ret}} + \lambda_{\text{att_obj}} (\mathcal{L}_{\text{att}} + \mathcal{L}_{\text{obj}}) + \lambda_{\text{sp}} \mathcal{L}_{\text{sp}}. \quad (12)$$

E. Inference

To predict the most likely attribute-object composition \hat{y} in a closed-world scenario, we select the label (a, o) from the test set $\mathcal{C}^{\text{test}}$ that maximizes the probability $p_{\text{sp}}(y = (a, o) | x; \theta)$:

$$\hat{y} = \arg \max_{(a, o) \in \mathcal{C}^{\text{test}}} p_{\text{sp}}(y = (a, o) | x; \theta), \quad (13)$$

where p_{sp} is computed following the same procedure in Eq. (8). Since the true attribute-object labels are unknown at inference, we construct text prompts for each $(a, o) \in \mathcal{C}^{\text{test}}$ using our learned prefix, and select the pair yielding the highest p_{sp} .

For open-world inference, \mathcal{C} expands to encompass all possible attribute-object pairs, making classification more

TABLE 1. Closed-World Results on MIT-States, UT-Zappos, and C-GQA. The results are reported for Seen (S), Unseen (U), Harmonic Mean (H), and Area Under the Curve (AUC). Bold and blue indicate the first and second best results, respectively.

Method	MIT-States				UT-Zappos				C-GQA			
	S	U	H	AUC	S	U	H	AUC	S	U	H	AUC
AoP [33]	14.3	17.4	9.9	1.6	59.8	54.2	40.8	25.9	17.0	5.6	5.9	0.7
LE+ [34]	15.0	20.1	10.7	2.0	53.0	61.9	41.0	25.7	18.1	5.6	6.1	0.8
TMN [35]	20.2	20.1	13.0	2.9	58.7	60.0	45.0	29.3	23.1	6.5	7.5	1.1
SymNet [19]	24.2	25.2	16.1	3.0	49.8	57.4	40.4	23.4	26.8	10.3	11.0	2.1
CompCos [32]	25.3	24.6	16.4	4.5	59.8	62.5	43.1	28.1	28.1	11.2	12.4	2.6
CGE [34]	28.7	25.3	17.2	5.1	56.8	63.6	41.2	26.4	28.7	25.3	17.2	5.1
Co-CGE [36]	32.1	28.3	20.0	6.6	62.3	66.3	48.1	33.9	33.3	14.9	14.4	4.1
SCEN [20]	29.9	25.2	18.4	5.3	63.5	63.1	47.8	32.0	28.9	25.4	17.5	5.5
CLIP [7]	30.2	40.0	26.1	11.0	15.8	49.1	15.6	5.0	7.5	25.0	8.6	1.4
CSP [23]	46.6	49.9	36.3	19.4	64.2	66.2	46.6	33.0	28.8	26.8	20.5	6.2
GIPCOL [11]	48.5	49.6	36.6	19.9	65.0	68.5	48.8	36.2	31.9	28.4	22.5	7.1
DFSP [13]	46.9	52.0	37.3	20.6	66.7	71.7	47.2	36.0	38.2	32.0	27.1	10.5
VAPS (Ours)	48.4	52.2	38.2	21.2	64.5	74.3	52.3	40.1	39.6	31.7	28.1	11.0

challenging. As in prior works [12], [13], [23], a feasibility calibration step is applied by computing a similarity score $p(a, o)$ for each candidate pair (a, o) . Any pair whose score falls below a threshold T is deemed infeasible and filtered out:

$$\hat{y} = \arg \max_{(a, o) \in \mathcal{C}, p(a, o) \geq T} p_{\text{sp}}(y = (a, o) \mid x; \theta). \quad (14)$$

This approach restricts the model to only consider attribute-object pairs deemed feasible. Selecting \hat{y} from the remaining pairs ensures that we capture the most probable composition for a given image, whether in a closed- or open-world setting.

V. Experiments and Results

A. Experimental Setup

Datasets. Our model is evaluated on three renowned CZSL datasets: MIT-States [37], UT-Zappos [38], and C-GQA [34]. MIT-States contains a variety of web-crawled images with 115 and 245 attributes and objects, respectively. 1262 seen compositions are used in training and 400 seen and unseen compositions used in testing. UT-Zappos is a smaller dataset containing images of 12 different types of shoes and 16 fine-grained attributes. C-GQA was built on top of the Stanford GQA dataset and contains a wide array of real life objects and attributes and possesses the most robust label space out of all three datasets, with over 800 seen and 900 unseen compositions in the test set.

Metrics. Following the setting of previous works [11], [13], [39], we assess our model’s performance using metrics to focus on both seen and unseen compositions. Specifically, we evaluate accuracy for *Seen (S)* and *Unseen (U)* compositions under both closed-world and open-world scenarios, as these two cases offer insights into the model’s generalization capabilities. We observe the *Harmonic Mean (H)* of the *S* and *U*

metrics. Given the inherent bias of zero-shot models toward seen compositions [15], [32], [40], the trade-off between seen and unseen performance is analyzed by plotting an accuracy curve across a bias range from $-\infty$ to $+\infty$. This allows us to compute the Area Under the Curve (AUC), the core metric reflecting the model’s overall capability.

Implementation Details. We utilize PyTorch 1.12.1 [42] for the implementation of our model. The model is optimized using the Adam optimizer over the previously mentioned datasets. Both the image encoder and text encoder are based on the pretrained CLIP ViT-L/14 model, and the entire model is trained and evaluated on a single NVIDIA A100 GPU. We set $M = 20$ for UT-Zappos and $M = 30$ for MIT-States and C-GQA, as the latter two datasets contain a wider variety of attribute-object compositions.

B. Comparison with State-of-the-Arts

Our method is compared to other state-of-the-art (SOA) CZSL methods, including: AoP [33], LE+ [34], TMN [35], SymNet [19], CompCos [32], CGE [34], Co-CGE [36], SCEN [20], CLIP [7], CSP [23], GIPCOL [11], and DFSP [13]. The same data splits are used across each model and are based using CLIP’s ViT-L/14 backbone.

The main results for the Closed-World setting are reported in Table 1. We can observe that VAPS outperforms all other SOA methods on the UT-Zappos dataset, specifically with an increase of 2.6% in classifying unseen compositions, a 5.0% increase in harmonic mean, and a 3.9% increase in AUC. When tested on the C-GQA dataset, our model demonstrates strength in seen accuracy with a 1.4% improvement, harmonic mean with a 1.0% increase and an increase in AUC to the previous SOA method by 0.5%, further showcasing its robust performance across the benchmarks. Additionally, VAPS remains competitive on MIT-States, delivering best

TABLE 2. Open-World Results on MIT-States, UT-Zappos, and CGQA. The results are reported for Seen (S), Unseen (U), Harmonic Mean (H), and Area Under the Curve (AUC). Bold and blue indicate the first and second best results, respectively.

Method	MIT-States				UT-Zappos				C-GQA			
	S	U	H	AUC	S	U	H	AUC	S	U	H	AUC
AoP [33]	16.6	5.7	4.7	0.7	50.9	34.2	29.4	13.7	-	-	-	-
LE+ [34]	14.2	2.5	2.7	0.3	60.4	36.5	30.5	16.3	19.2	0.7	1	0.1
TMN [35]	12.6	0.9	1.2	0.1	55.9	18.1	21.7	8.4	-	-	-	-
SymNet [19]	21.4	7	5.8	0.8	53.3	44.6	34.5	18.5	26.7	2.2	3.3	0.4
CompCos [32]	25.4	10.0	8.9	1.6	59.3	46.8	36.9	21.9	-	-	-	-
CGE [34]	32.4	5.1	6.0	1.0	61.7	47.7	39.0	23.1	26.7	2.2	3.3	0.5
Co-CGE [36]	30.3	11.2	10.7	2.3	61.1	45.8	40.8	23.3	32.1	3.0	4.8	0.8
KG-SP [41]	28.4	7.5	7.4	1.3	61.8	52.1	42.3	26.5	31.5	2.9	4.7	0.8
CLIP [7]	30.1	14.3	12.8	3.0	15.7	20.6	11.6	2.2	7.5	4.6	4.0	0.3
CSP [23]	46.3	15.7	17.4	5.7	64.1	44.1	38.9	22.7	28.7	5.2	6.9	1.2
GIPCOL [11]	48.5	16.0	17.9	6.3	65.0	45.0	40.1	23.5	31.6	5.5	7.3	1.3
DFSP [13]	47.5	18.5	19.3	6.8	66.8	60.0	44.0	30.3	38.3	7.2	10.4	2.4
VAPS (Ours)	48.3	18.2	20.0	7.0	64.4	60.1	47.8	31.7	39.5	7.3	10.8	2.6

results in seen, unseen, and AUC. Table 2 showcases the results for the more challenging open-world scenario. An improved unseen accuracy, harmonic mean, and AUC can be observed UT-Zappos, while all metrics seen increases across CGQA. Once again, an increase in harmonic mean and AUC is shown on the MIT-States dataset. We can attribute this success to the use of the visual prompt repository, which leverages learned visual semantics from the image encoder, as well as the prompt adapter, which shifts the soft prompt prefix for each individual image. Previous methods disregard enhancing the visual features from the image encoder while also assuming that one learned soft prompt prefix can generalize to all compositions. These outcomes emphasize the effectiveness of VAPS in both closed and open-world scenarios, where its visual prompt retrieval mechanism and soft prompt prefix adaptation results in consistent gains over all datasets against competing methods.

C. Ablation Study

To better understand the behavior of our model, we begin by conducting an ablation study to assess the contribution of each component branch. Additionally, we explore how varying the number of selected prompts from the visual repository affects performance. This study is performed on the UT-Zappos and MIT-States datasets.

Component Study. We analyze how different branches interact in the proposed model in both closed-world and open-world settings in Table 3. Specifically, we examine different permutations of cross-attention (*ca*), prompt adapter (*pa*), and prompt repository (*pr*). All configurations are kept consistent throughout each experiment. When the *pa* branch is excluded from the model, a decrease across all metrics is observed when compared to the full model. Over a 2% decrease occurs on the seen and unseen composition accuracy and AUC drops 1.6% on UT-Zappos in the open-world

TABLE 3. Ablation of different model components and its effect on performance on Closed World (CW) and Open World (OW). Bold represents the best results.

	Components			MIT-States				UT-Zappos			
	<i>pr</i>	<i>ca</i>	<i>pa</i>	S	U	H	AUC	S	U	H	AUC
CW	✓	✓	✓	48.4	52.2	38.2	21.2	64.5	74.3	52.3	40.1
	✓	✓		47.9	51.5	37.3	20.5	62.2	72.1	52.2	38.5
	✓		✓	48.5	51.6	37.6	20.8	60.7	69.7	50.1	36.0
		✓	✓	48.3	18.2	20.0	7.0	64.4	60.1	47.8	31.7
OW	✓	✓		48.8	17.4	19.2	6.6	64.0	53.5	44.2	28.0
		✓	✓	48.7	17.5	19.5	6.8	61.8	53.2	43.0	26.9

setting. For the closed-world setting, a decrease of 6.6% and 3.7% occur across unseen accuracy and AUC, respectively. Similarly, a decrease across all metrics occur on MIT-States when removing the *pa* branch. Next, an ablation is performed to study the effect of the prompt repository by keeping only *ca* and *pa*. When removing *pr*, all metrics decrease across the UT-Zappos dataset for both closed and open world scenarios. On MIT-States, a slight decrease of 0.4% in AUC occurs; however, seen accuracy increases slightly by 0.1%. Overall, a higher variability occurs in the results across the UT-Zappos dataset when ablating components compared to MIT-States. Retaining the prompt repository alongside the cross-attention and prompt adapter components ensures optimal performance, particularly in complex open-world scenarios. Furthermore, retaining all three branches of the model ensures that the core AUC metric remains at its highest level.

Repository Size and Number of Selected Prompts. This study experiments with initiating the size of the repository and the number of selected prompts with different values. Through empirical analysis, it was observed the optimal vi-

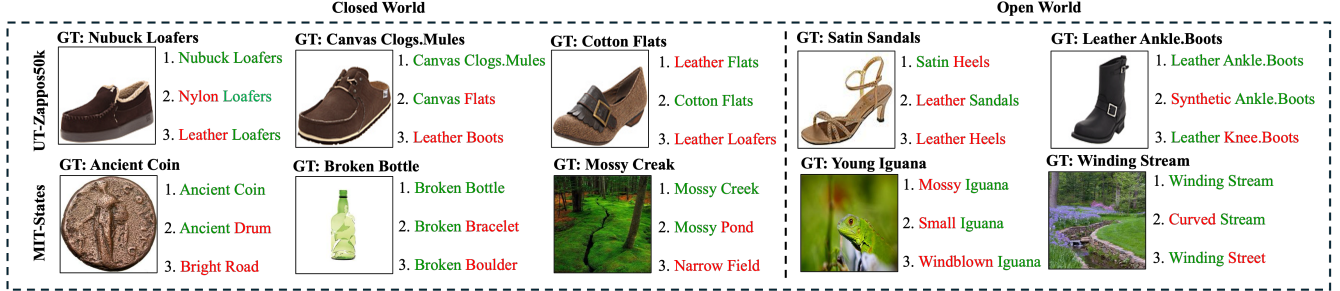


FIGURE 4. Top-3 qualitative results. Each example displays the ground truth (GT) label and predictions, highlighting correct predictions in green and incorrect ones in red.

sual repository size was between 20 and 30 prompts for each dataset. This range offers a sufficient diversity of learned prompts. Additionally, our analysis showed that selecting a single visual prompt for attributes and one for objects per image was optimal for compositional disentanglement. Our results show some variability between datasets. On MIT-States, increasing the repository size slightly improves harmonic mean and AUC, suggesting that a moderate diversity of prompts supports its range of compositions. For UT-Zappos, smaller repository sizes and selecting two prompts per image yield more noticeable AUC gains, likely due to one prompt representing attributes and one per image. This demonstrates that while both datasets benefit from the prompt repository, optimal configurations vary with dataset characteristics, showcasing the adaptability of our approach across different compositional settings.

D. Qualitative Results

To observe the robustness of our method, the top-3 qualitative results for selected images across UT-Zappos and MIT-States datasets are reported for both closed and open world settings, shown in Figure 4. For example, our model successfully classifies images of 'Nubuck Loafers' and 'Canvas Clogs' with the first prediction, but classifies 'Cotton Flats' correctly in the second prediction. However, the first prediction for 'Cotton Flats' was 'Leather Flats', which may be due to the brown color of the flats in the studied image. Similar results also occur in the MIT-States and UT-Zappos datasets. Our model correctly classifies all three of the images from MIT-States with its first prediction. For the 'Ancient Coin' image, despite the challenging visual similarities it may have with objects such as 'Ancient Drum', the model demonstrates strong attribute recognition by correctly identifying the 'Ancient' attribute, which helps it correctly classify the object. Similarly, for the 'Broken Bottle' image, although the texture and overall form might overlap with objects like 'Broken Boulder', the model effectively uses the 'Broken' attribute as a distinguishing feature, allowing it to make informed predictions.

Our model's robustness is further demonstrated in the open world setting. For instance, it successfully differentiates between visually similar but distinct material, such as 'Leather' and 'Synthetic', when classifying 'Ankle Boots'. Similarly,

TABLE 4. Comparison of datasets with varying repository size and number of selected prompts in closed-world setting.

Rep. Size	Selected N	MIT-States				UT-Zappos			
		S	U	H	AUC	S	U	H	AUC
20	2	49.2	50.5	37.2	20.5	64.5	74.3	52.3	40.1
20	4	49.3	50.4	37.1	20.6	64.4	70.1	47.1	35.1
30	2	48.4	52.2	38.2	21.2	62.4	72.3	49.9	36.9
30	4	48.5	52.1	38.2	20.8	61.0	72.6	49.3	35.8

the model was able to classify the image of the 'Winding Stream' with high accuracy. However, some incorrect first predictions are seen in each dataset, such as predicting the image of the 'Iguana' as 'Mossy' instead of 'Young'. Also, the prediction of a 'Windblown Iguana' highlights the challenge posed by the open-world scenario since this attribute is not plausible for the given object. Overall, these qualitative results represent the effectiveness of our method in both closed and open world settings. By focusing on key object features and attribute details, our model is able to make accurate classifications, even when confronted with unseen compositions or visually complex scenarios.

VI. Conclusion

In this paper, we propose a Visual Adaptive Prompting System (VAPS) to bridge the gap between semantic and visual features for CZSL. By leveraging a dynamic visual prompt repository and a similarity-based retrieval mechanism to select relevant visual prompts based on attribute and objects, VAPS enhances the model's ability to generalize to unseen compositions. Furthermore, we propose dynamically adapting the learnable prompt prefix based on the image features derived from CLIP's image encoder. Our experiments on benchmark datasets demonstrate that VAPS achieves state-of-the-art performance on metrics across the UT-Zappos and CQGA datasets, highlighting its capability to disentangle and recompose visual features effectively. This work paves the way for more robust VLM's in compositional reasoning tasks.

REFERENCES

- [1] B. M. Lake, "Towards more human-like concept learning in machines: Compositionality, causality, and learning-to-learn," Ph.D. dissertation, Massachusetts Institute of Technology, 2014.
- [2] B. M. Lake, T. D. Ullman, J. B. Tenenbaum, and S. J. Gershman, "Building machines that learn and think like people," *Behavioral and*

brain sciences, vol. 40, p. e253, 2017.

[3] S. M. Frankland and J. D. Greene, “Concepts and compositionality: in search of the brain’s language of thought,” *Annual review of psychology*, vol. 71, no. 1, pp. 273–303, 2020.

[4] S. Hao, K. Han, and K.-Y. K. Wong, “Learning attention as disentangler for compositional zero-shot learning,” in *Proceedings of the IEEE/CVF Conference on Computer Vision and Pattern Recognition*, 2023, pp. 15 315–15 324.

[5] D. Huynh and E. Elhamifar, “Fine-grained generalized zero-shot learning via dense attribute-based attention,” in *Proceedings of the IEEE/CVF Conference on Computer Vision and Pattern Recognition*, 2020, pp. 4483–4493.

[6] M. Yang, C. Xu, A. Wu, and C. Deng, “A decomposable causal view of compositional zero-shot learning,” *IEEE Transactions on Multimedia*, vol. 25, pp. 5892–5902, 2022.

[7] A. Radford, J. W. Kim, C. Hallacy, A. Ramesh, G. Goh, S. Agarwal, G. Sastry, A. Askell, P. Mishkin, J. Clark *et al.*, “Learning transferable visual models from natural language supervision,” in *International conference on machine learning*. PMLR, 2021, pp. 8748–8763.

[8] S. Jin, X. Jiang, J. Huang, L. Lu, and S. Lu, “Llms meet vlms: Boost open vocabulary object detection with fine-grained descriptors,” *arXiv preprint arXiv:2402.04630*, 2024.

[9] W. Jin, Y. Cheng, Y. Shen, W. Chen, and X. Ren, “A good prompt is worth millions of parameters: Low-resource prompt-based learning for vision-language models,” *arXiv preprint arXiv:2110.08484*, 2021.

[10] K. Zhou, J. Yang, C. C. Loy, and Z. Liu, “Learning to prompt for vision-language models,” *International Journal of Computer Vision*, vol. 130, no. 9, pp. 2337–2348, 2022.

[11] G. Xu, J. Chai, and P. Kordjamshidi, “Gipcol: Graph-injected soft prompting for compositional zero-shot learning,” in *Proceedings of the IEEE/CVF Winter Conference on Applications of Computer Vision*, 2024, pp. 5774–5783.

[12] W. Bao, L. Chen, H. Huang, and Y. Kong, “Prompting language-informed distribution for compositional zero-shot learning,” *arXiv preprint arXiv:2305.14428*, 2023.

[13] X. Lu, S. Guo, Z. Liu, and J. Guo, “Decomposed soft prompt guided fusion enhancing for compositional zero-shot learning,” in *Proceedings of the IEEE/CVF Conference on Computer Vision and Pattern Recognition*, 2023, pp. 23 560–23 569.

[14] L. Ma, Q. Sun, S. Georgoulis, L. Van Gool, B. Schiele, and M. Fritz, “Disentangled person image generation,” in *Proceedings of the IEEE conference on computer vision and pattern recognition*, 2018, pp. 99–108.

[15] S. Min, H. Yao, H. Xie, C. Wang, Z.-J. Zha, and Y. Zhang, “Domain-aware visual bias eliminating for generalized zero-shot learning,” in *Proceedings of the IEEE/CVF Conference on Computer Vision and Pattern Recognition*, 2020, pp. 12 664–12 673.

[16] B. Tong, C. Wang, M. Klinkigt, Y. Kobayashi, and Y. Nonaka, “Hierarchical disentanglement of discriminative latent features for zero-shot learning,” in *Proceedings of the IEEE/CVF Conference on Computer Vision and Pattern Recognition (CVPR)*, June 2019.

[17] Z. Chen, Y. Luo, R. Qiu, S. Wang, Z. Huang, J. Li, and Z. Zhang, “Semantics disentangling for generalized zero-shot learning,” in *Proceedings of the IEEE/CVF international conference on computer vision*, 2021, pp. 8712–8720.

[18] X. Li, Z. Xu, K. Wei, and C. Deng, “Generalized zero-shot learning via disentangled representation,” in *Proceedings of the AAAI Conference on Artificial Intelligence*, vol. 35, no. 3, 2021, pp. 1966–1974.

[19] Y.-L. Li, Y. Xu, X. Mao, and C. Lu, “Symmetry and group in attribute-object compositions,” in *Proceedings of the IEEE/CVF Conference on Computer Vision and Pattern Recognition*, 2020, pp. 11 316–11 325.

[20] X. Li, X. Yang, K. Wei, C. Deng, and M. Yang, “Siamese contrastive embedding network for compositional zero-shot learning,” in *Proceedings of the IEEE/CVF Conference on Computer Vision and Pattern Recognition*, 2022, pp. 9326–9335.

[21] C. Jing, Y. Li, H. Chen, and C. Shen, “Retrieval-augmented primitive representations for compositional zero-shot learning,” in *Proceedings of the AAAI Conference on Artificial Intelligence*, vol. 38, no. 3, 2024, pp. 2652–2660.

[22] Q. Wang, L. Liu, C. Jing, H. Chen, G. Liang, P. Wang, and C. Shen, “Learning conditional attributes for compositional zero-shot learning,” in *Proceedings of the IEEE/CVF Conference on Computer Vision and Pattern Recognition*, 2023, pp. 11 197–11 206.

[23] N. V. Nayak, P. Yu, and S. H. Bach, “Learning to compose soft prompts for compositional zero-shot learning,” *arXiv preprint arXiv:2204.03574*, 2022.

[24] P. Liu, W. Yuan, J. Fu, Z. Jiang, H. Hayashi, and G. Neubig, “Pre-train, prompt, and predict: A systematic survey of prompting methods in natural language processing,” *ACM Computing Surveys*, vol. 55, no. 9, pp. 1–35, 2023.

[25] M. U. Khattak, H. Rasheed, M. Maaz, S. Khan, and F. S. Khan, “Maple: Multi-modal prompt learning,” in *Proceedings of the IEEE/CVF Conference on Computer Vision and Pattern Recognition*, 2023, pp. 19 113–19 122.

[26] C. Shi and S. Yang, “Logoprompt: Synthetic text images can be good visual prompts for vision-language models,” in *Proceedings of the IEEE/CVF International Conference on Computer Vision*, 2023, pp. 2932–2941.

[27] A. Ramesh, M. Pavlov, G. Goh, S. Gray, C. Voss, A. Radford, M. Chen, and I. Sutskever, “Zero-shot text-to-image generation,” in *International conference on machine learning*. PMLR, 2021, pp. 8821–8831.

[28] W. Kim, B. Son, and I. Kim, “Vilt: Vision-and-language transformer without convolution or region supervision,” in *International conference on machine learning*. PMLR, 2021, pp. 5583–5594.

[29] T. Huang, J. Chu, and F. Wei, “Unsupervised prompt learning for vision-language models,” *arXiv preprint arXiv:2204.03649*, 2022.

[30] Z. Wang, Z. Zhang, C.-Y. Lee, H. Zhang, R. Sun, X. Ren, G. Su, V. Perot, J. Dy, and T. Pfister, “Learning to prompt for continual learning,” in *Proceedings of the IEEE/CVF Conference on Computer Vision and Pattern Recognition*, 2022, pp. 139–149.

[31] K. Zhou, J. Yang, C. C. Loy, and Z. Liu, “Conditional prompt learning for vision-language models,” in *Proceedings of the IEEE/CVF Conference on Computer Vision and Pattern Recognition*, 2022, pp. 16 816–16 825.

[32] M. Mancini, M. F. Naeem, Y. Xian, and Z. Akata, “Open world compositional zero-shot learning,” in *Proceedings of the IEEE/CVF Conference on Computer Vision and Pattern Recognition*, 2021, pp. 5222–5230.

[33] T. Nagarajan and K. Grauman, “Attributes as operators: factorizing unseen attribute-object compositions,” in *Proceedings of the European Conference on Computer Vision (ECCV)*, 2018, pp. 169–185.

[34] M. F. Naeem, Y. Xian, F. Tombari, and Z. Akata, “Learning graph embeddings for compositional zero-shot learning,” in *Proceedings of the IEEE/CVF Conference on Computer Vision and Pattern Recognition*, 2021, pp. 953–962.

[35] S. Purushwalkam, M. Nickel, A. Gupta, and M. Ranzato, “Task-driven modular networks for zero-shot compositional learning,” in *Proceedings of the IEEE/CVF International Conference on Computer Vision*, 2019, pp. 3593–3602.

[36] M. Mancini, M. F. Naeem, Y. Xian, and Z. Akata, “Learning graph embeddings for open world compositional zero-shot learning,” *IEEE Transactions on pattern analysis and machine intelligence*, vol. 46, no. 3, pp. 1545–1560, 2022.

[37] P. Isola, J. J. Lim, and E. H. Adelson, “Discovering states and transformations in image collections,” in *Proceedings of the IEEE conference on computer vision and pattern recognition*, 2015, pp. 1383–1391.

[38] A. Yu and K. Grauman, “Fine-grained visual comparisons with local learning,” in *Proceedings of the IEEE conference on computer vision and pattern recognition*, 2014, pp. 192–199.

[39] Y. Li, Z. Liu, H. Chen, and L. Yao, “Context-based and diversity-driven specificity in compositional zero-shot learning,” in *Proceedings of the IEEE/CVF Conference on Computer Vision and Pattern Recognition*, 2024, pp. 17 037–17 046.

[40] W.-L. Chao, S. Changpinyo, B. Gong, and F. Sha, “An empirical study and analysis of generalized zero-shot learning for object recognition in the wild,” in *Computer Vision–ECCV 2016: 14th European Conference, Amsterdam, The Netherlands, October 11–14, 2016, Proceedings, Part II 14*. Springer, 2016, pp. 52–68.

[41] S. Karthik, M. Mancini, and Z. Akata, “Kg-sp: Knowledge guided simple primitives for open world compositional zero-shot learning,” in *Proceedings of the IEEE/CVF Conference on Computer Vision and Pattern Recognition*, 2022, pp. 9336–9345.

[42] A. Paszke, S. Gross, F. Massa, A. Lerer, J. Bradbury, G. Chanan, T. Killeen, Z. Lin, N. Gimelshein, L. Antiga *et al.*, “Pytorch: An imperative style, high-performance deep learning library,” *Advances in neural information processing systems*, vol. 32, 2019.